Elastic interpretation of the glass transition in aluminosilicate liquids

Morten M. Smedskjaer, Liping Huang, Garth Scannell, and John C. Mauro

Phys. Rev. B **85**, 144203 — Published 27 April 2012

DOI: 10.1103/PhysRevB.85.144203

On the Elastic Interpretation of the Glass Transition in Aluminosilicate Liquids

Morten M. Smedskjaer,[1] Liping Huang,[2] Garth Scannell,[2] John C. Mauro[1,*]

[1] *Science and Technology Division, Corning Incorporated, Corning, NY 14831, USA*

[2] *Department of Materials Science and Engineering, Rensselaer Polytechnic Institute, Troy, NY 12180, USA*

* Corresponding author: Tel: +1 607-974-2185. E-mail: mauroj@corning.com.

ABSTRACT

One of the remaining puzzles of the glass transition is the origin of a glass-forming liquid's "fragility," which quantifies the departure of its relaxation time from Arrhenius activated kinetics. According to the shoving model proposed by Dyre, fragility is controlled by the instantaneous shear modulus of the liquid, since any flow event requires a local volume increase and the related activation energy is equal to the work done in shoving aside the surrounding atoms. Here, we present an *in situ* high-temperature Brillouin spectroscopy test of the shoving model near the glass transition of eight aluminosilicate glass-forming systems. We find that the measured viscosity data agree qualitatively with the measured temperature dependence of shear moduli, as predicted by the shoving model. However, the model systematically under-predicts the values of fragility for our aluminosilicate liquids. This suggests that the dynamics of the glass transition are governed by additional factors beyond the evolution of the shear modulus, such as configurational entropy. We have also compared the glass transition temperature $T_{g,vis}$ obtained from viscosity (temperature at 10^{12} Pa s) with the onset temperatures of the decrease in elastic moduli ($T_{g,elas}$) and increase in the thermal expansion coefficient ($T_{g,CTE}$) during heating. While we find an approximate one-to-one correlation between $T_{g,vis}$ and $T_{g,CTE}$, it is clear that the elastic moduli probe a different frequency response of the glass structure since $T_{g,elas}$ is systematically lower than $T_{g,vis}$.

I. INTRODUCTION

The physics of glass-forming liquids and the glasses into which they solidify is a topic attracting widespread attention [1-10]. At the heart of this problem lies the glass transition, i.e., the process by which an equilibrium, ergodic liquid is gradually frozen into a nonequilibrium, nonergodic glassy state [11-14]. The most fascinating feature of a supercooled glass-forming liquid is arguably its dramatic rise in viscosity (η) or relaxation time (τ) as it is cooled toward the glass transition. For most liquids, the temperature dependence of η and τ is super-Arrhenius, i.e., η and τ increase more dramatically upon cooling than expected from an Arrhenius law [15-19]. In other words, the free energy activation energy barrier to viscous flow is not a constant, but rather dependent on temperature [20-26]. The glass transition and the non-Arrhenius behavior are still considered as major scientific challenges in the condensed matter physics community.

The glass transition temperature (T_g) is the characteristic temperature of a liquid indicating the onset of the glass transition. However, the value of T_g depends on both its definition and on the method of determination. Consequently, different T_g values are often found in literature for the same glass composition. Following the convention of Angell [6-8], the most common definition of T_g is the isokom temperature at which the equilibrium shear viscosity is equal to 10^{12} Pa s ($T_{g,vis}$) [27]. The glass transition also involves major changes in second-order thermodynamics properties such as heat capacity [28-30] and compressibility [31,32]. In particular, the change in isobaric heat capacity (C_p) during the glass transition has been intensively examined using differential scanning calorimetry (DSC) [33-39]. C_p increases when heating through the glass transition since the glassy state at low temperature contains primarily vibrational degrees of freedom, whereas the liquid state at high temperature contains both vibrational and configurational degrees of freedom. Yue [33,34] has shown that $T_{g,vis}$ is in accordance with the onset temperature of the glass transition measured calorimetrically at downscan and upscan rates of 10 °C/min.

Other properties exhibiting changes during the glass transition include thermal expansion and elastic moduli. The thermal expansion behavior of glass is technologically very important, since it is often desirable to match the coefficient of thermal expansion (CTE) of a glass to another coupled material or to simply minimize the thermal expansion to reduce dimensional changes [40]. Potuzak *et al.* [41,42] have recently

demonstrated that the CTE of a glass-forming liquid can be separated into additive vibrational and configurational contributions, i.e., the CTE increases during heating through the glass transition similarly to the increase of C_p during the glass transition. The elastic moduli of glasses are important mechanical properties, intimately linked with the atomic packing of the glassy network [43]. As the glass softens during heating, the elastic moduli generally decrease (notwithstanding a few notable exceptions [44]) and the softening rate depends on the level of cooperativity of atomic movements [43,45]. During the glass transition, the elastic moduli can exhibit different rates of change with temperature [46].

Several models have been proposed to elucidate the non-Arrhenius behavior of η and τ [17,47-50]. As the elastic properties are correlated with the short- and intermediate range order [43], here we consider the phenomenological "shoving model" of Dyre *et al.* [51-55], in which the dynamics of the glass-forming liquid are considered to be controlled by the elasticity through the instantaneous (infinite frequency) shear modulus G_∞. According to the shoving model, the non-Arrhenius scaling of relaxation time (i.e., the fragility) is controlled by the temperature dependence of G_∞. The shear viscosity and relaxation time are related via Maxwell's equation,

$$\tau = \frac{\eta}{G_\infty}. \tag{1}$$

G_∞ increases as temperature decreases, but its temperature dependence is insignificant compared to the dramatic temperature dependencies of η and τ, i.e., η and τ are roughly proportional. The shoving model assumes that the activation barrier for viscous flow has two contributions: (i) rearrangements of molecules or structural units, when a thermal fluctuation leads to extra space being created locally; (ii) "shoving" aside the surrounding liquid to reduce the first contribution. According to the shoving model, the main contribution comes from (ii), i.e., the activation energy is mainly elastic energy [5]. On a short time scale, the liquid behaves as a solid with elastic moduli equal to the instantaneous elastic moduli. Furthermore, it is assumed that all flow events possess spherical symmetry, i.e., the surroundings are subject to a pure shear displacement and not associated with any density change [5,51,56]. Since this displacement happens on a short time scale, the shoving work is proportional to the instantaneous shear modulus, which leads to the following expression for the relaxation time [51]:

$$\tau(T) = \tau_0 \exp\left[\frac{G_\infty(T)V_c}{k_B T}\right], \quad (2)$$

where τ_0 is the microscopic time, k_B is Boltzmann's constant, and V_c is a characteristic microscopic volume, which is assumed to be temperature independent. It follows from Eq. (2) that the non-Arrhenius behavior arises due to the temperature dependence of G_∞. Hence, V_c is the proportionality constant between $G_\infty(T)$ and the activation barrier to viscous flow ($\Delta F(T)$),

$$\Delta F(T) = G_\infty(T)V_c\,. \quad (3)$$

While the shoving model has been experimentally supported by data for various organic [51,54,57,58] and metallic [59,60] glass-forming systems, to the best of our knowledge the model has not yet been tested for oxide systems. Recent molecular-dynamics simulations of a model polymer system also revealed an absence of correlations between the instantaneous elasticity and the structural relaxation [61]. Please note that in Eqs. (2) and (3) we have written the relaxation time and activation barrier as functions of temperature only. In general these can also be functions of volume, pressure, thermal history, pressure history, etc. Here we restrict our attention to the temperature dependence of relaxation time under isobaric conditions.

In this work, we address the validity of the shoving model in oxide systems by performing high-temperature *in situ* Brillouin spectroscopy measurements to determine the temperature dependence of G_∞ and compare it with the measured temperature dependence of shear viscosity. We perform these measurements on various sodium aluminosilicate glasses with CaO and/or MgO that have been designed in a way to span a wide range of glass transition temperatures (from about 500 to 800 °C). We also investigate how the glass transition temperatures obtained from the high-temperature elastic moduli data compare with those obtained from high-temperature thermal expansion and viscosity data. Hence, this study will also shed light on the structural and topological changes occurring during the glass transition and how it manifests itself in different macroscopic glass properties.

II. EXPERIMENTAL PROCEDURE

The nominal compositions (in mol%) of the glasses under study are (76-x)SiO_2 – x Al_2O_3 – 16 Na_2O – 8 MO with x = 0, 2.7, 5.3, 8, 10.7, 13.3, 16, 18.7, 21.3, and 24 for M = Mg, Ca. In addition, for x = 16, four glasses with different [MgO]/[CaO] ratios equal to 0.25, 0.67, 1.5, and 4 were prepared [62]. All glasses included ~0.15 mol% SnO_2 as a fining agent. To prepare the glasses, the mixed batch materials were first melted in a covered platinum crucible for 5 h in air at a temperature between 1450 and 1600 °C depending on composition. In order to ensure chemical homogeneity, the melts were first quenched in water, and then the resulting glass pieces were crushed and remelted for 6 h at 1650 ºC and finally poured in air. The glasses were annealed for 2 h at their respective annealing points. The chemical compositions of the final glasses were determined using x-ray fluorescence. The analyzed compositions were within 0.5 mol% of the nominal ones. Room temperature densities of the glasses were determined using Archimedes' principle.

The temperature dependence of equilibrium viscosity was measured by performing beam bending, parallel plate, and concentric cylinder experiments. The viscosity curve of each composition is represented by data points at $10^{6.6}$ Pa s (the softening point, obtained via parallel plate viscometry), 10^{11} Pa s (obtained via beam bending viscometry), and 12-20 data points in the range of 10 to 10^6 Pa s (obtained via the concentric cylinder method). For beam bending experiments, bars of 5.5 cm length and 2.5 × 2.5 mm^2 cross-section were cut from the bulk glasses. For parallel plate experiments, cylinders of 6 mm diameter and 5 mm thickness were core-drilled and afterwards the flats were polished to an optical finish. For concentric cylinder experiments, ~600 g of crushed glass was remelted. The errors associated with determining the 10^{11} Pa s point by the beam bending method and the $10^{6.6}$ Pa s point by the parallel plate method are ±1 and ±2°C, respectively. The estimated error in viscosity for the high-temperature measurements (by the concentric cylinder method) is $\Delta \log \eta = \pm 0.02$ (η in Pa s).

The high-temperature thermal expansion measurements were performed as described in Ref. [41]. A constant heating rate of 30 °C/min was employed. CTE values will be quoted for linear thermal expansion (volume expansion coefficients are a factor of three larger, since the glasses are isotropic).

The high-temperature elastic moduli were determined by Brillouin light scattering experiments on eight of the glasses (x = 0, 8, 16, and 24 for M = Ca and Mg). The measurements were performed on samples that were optically polished to 50-80 μm in thickness with two parallel top and bottom surfaces by using 600 grit SiC sand paper and cerium oxide slurry. To monitor the evolution of elastic properties as a function of temperature, the polished thin samples were heated up in a Linkham TS1500 heating stage from room temperature to the maximum temperature with the coefficient of thermal expansion data and room temperature density available for each composition. Brillouin scattering measurements were taken through the top fused quartz window of the heating stage in air. A six-pass high contrast Fabry-Perot interferometer from JSR Scientific Instruments was used to carry out the *in situ* high-temperature light scattering experiments. This was done by using a 532 nm Verdi V2 DPSS green laser as the probing light source. In all experiments, a heating rate of 50 °C/min was used. After each temperature was reached, Brillouin spectra were taken after the temperature inside the heating stage had stabilized for 10 minutes. By measuring the frequency shift of the longitudinal and transverse modes, the corresponding velocities for longitudinal (V_L) and transverse acoustic waves (V_T) can be calculated by

$$V_L = \frac{\Delta f_L \lambda}{2\sin\theta} \tag{4}$$

and

$$V_T = \frac{\Delta f_T \lambda}{2\sin\theta}, \tag{5}$$

where Δf_L and Δf_T are the frequency shift for the longitudinal and transverse modes, respectively, λ is the laser wavelength of 532 nm, and θ is the scattering angle in the platelet geometry. The measured sound velocities V_L and V_T, combined with the density ρ calculated from the coefficient of thermal expansion, were used to calculate the temperature dependence of the elastic moduli via the elastic constants C_{11} and C_{44} and the following equations:

$$C_{11} = \rho V_L^2, \tag{6}$$

$$C_{44} = \rho V_T^2, \tag{7}$$

$$E = C_{44}\frac{3C_{11} - 4C_{44}}{C_{11} - C_{44}}, \tag{8}$$

$$B = \frac{3C_{11} - 4C_{44}}{3}, \tag{9}$$

$$G = C_{44}, \tag{10}$$

and

$$\nu = \frac{E}{2G} - 1, \tag{11}$$

where E is Young's modulus, B is the bulk modulus, G is the shear modulus, and ν is Poisson's ratio.

III. RESULTS

A. Viscosity data

There exist various models for fitting and describing the temperature dependence of viscosity [15,18,22]. Here we employ a recently proposed model by Mauro *et al.* [19] that is derived from topological constraint theory [63] and provides realistic extrapolations of configurational entropy at both the low and high temperature limits. The model is named MYEGA after its inventors (Mauro-Yue-Ellison-Gupta-Allan) and it can be written in terms of $T_{g,vis}$ and Angell's liquid fragility index m [64] as [19],

$$\log_{10}\eta(T) = \log_{10}\eta_\infty + (12 - \log_{10}\eta_\infty)\frac{T_{g,vis}}{T}\exp\left[\left(\frac{m}{12 - \log_{10}\eta_\infty} - 1\right)\left(\frac{T_{g,vis}}{T} - 1\right)\right], \tag{12}$$

where η_∞ is the high-temperature limit of the liquid viscosity [65-67], and T is the absolute temperature. We have fit Eq. (12) to the viscosity data of the twenty-four glass forming liquids using a Levenberg-Marquardt algorithm [68,69] to obtain $T_{g,vis}$ for each composition. As an example, Figure 1(a) shows the temperature dependence of logarithmic viscosity for the glass with x = 0 and M = Ca. Figure 1(b) shows the composition dependence of $T_{g,vis}$. $T_{g,vis}$ increases with increasing Al_2O_3 content for both the Ca- and Mg-glasses, and for x = 16, $T_{g,vis}$ increases with increasing degree of substitution of MgO for CaO (inset of Fig. 1(b)). The structural origins of these composition dependences will be discussed elsewhere.

B. Brillouin light scattering data

Young's modulus (E) for eight selected glasses is shown as a function of temperature in Figure 2. We have found similar temperature dependence of shear and bulk moduli, as shown in Figure 3 for shear modulus. At room temperature, the elastic moduli increase with increasing concentration of Al_2O_3 for both Ca- and Mg-glasses. With increasing temperature, the elastic moduli decrease, but this occurs very gradually up to the glass transition. Above the glass transition, the elastic moduli decrease very rapidly with temperature and the glass transition is marked by a discontinuity in the temperature dependence of elastic moduli. Hence, we define the glass transition temperature from the Brillouin experiments ($T_{g,elas}$) as the intersection point between the tangent lines of $G(T)$ below and above the glass transition. The procedure for determining $T_{g,elas}$ is illustrated in Figure 4(a) by using the glass with $x = 0$ and M = Ca as an example. Figure 4(b) shows the composition dependence of $T_{g,elas}$. In qualitative agreement with the $T_{g,vis}$ data, $T_{g,elas}$ increases with increasing $[Al_2O_3]$ for both series.

Figure 5 shows the composition and temperature dependence of Poisson's ratio (v), the negative of the ratio of transverse contraction strain to longitudinal extension strain in the direction of elastic loading. The Poisson's ratio at room temperature increasing with increasing $[Al_2O_3]$ for both the Ca- and Mg-containing glasses (Fig. 5(a)). Furthermore, as the elastic properties are sensitive to temperature, so is the Poisson's ratio and we find that v increases with increasing temperature toward that of an incompressible fluid ($v = 0.5$), as shown in Figure 5(b). In Figure 5(c), we have plotted the slope of the v vs. T curve (dv/dT) as a function of $[Al_2O_3]$ for the two series of glasses. dv/dT decreases with increasing alumina content.

C. Thermal expansion data

Figure 6(a) shows an example of the high-temperature thermal expansion data obtained in this work. The data are for the glass with $x = 0$ and M = Ca. The glass expands during heating, but the rate of change in expansion with temperature increases during the glass transition. This is directly seen from the temperature dependence of the instantaneous coefficient of thermal expansion (CTE). We have determined the glass transition temperature based on these measurements ($T_{g,CTE}$) as the intersection point between the straight lines of the expansion curve below and above the glass transition (Fig. 6(a)). $T_{g,CTE}$ increases with increasing

[Al_2O_3] for both the Ca- and Mg-glasses, and for x = 16, $T_{g,CTE}$ increases with increasing degree of substitution of MgO for CaO (Fig. 6(b)).

IV. DISCUSSION

A. Comparison of glass transition temperatures

In the following, we discuss the connection among the three measures of glass transition temperature ($T_{g,vis}$, $T_{g,elas}$, and $T_{g,CTE}$) and their relation to structural changes associated with the glass transition. As shown in Figure 7(a), $T_{g,CTE}$ and $T_{g,vis}$ exhibit a strong linear correlation (R^2 = 0.996). $T_{g,CTE}$ was determined at rate of 30 °C/min, and Yue [33,34] has shown that $T_{g,vis}$ agrees with the calorimetric glass transition temperature measured at 10 °C/min (when subjected to a prior downscan also at 10 °C/min). However, we find that $T_{g,CTE}$ is on average smaller by ~10 °C than $T_{g,vis}$, and apparently $T_{g,CTE}$ and $T_{g,vis}$ decouple to an increasing extent with increasing Al_2O_3 content.

The rapid decrease in elastic moduli during heating through the glass transition is a direct consequence of the structural degradation. At low temperature, atomic mobility is low and the glass structures are able to store a large amount of energy elastically. At higher temperatures, the mobility of small structural regimes becomes activated and the structure expands due to the increased thermal motions. Thus, the glass is able to store less energy elastically and the moduli decrease. The rate of degradation of elastic moduli has previously been shown to be well correlated with the fragility index m, i.e., the rate of the increase in viscosity during cooling [43-46]. It could therefore be expected that there also exists a strong correlation between $T_{g,vis}$ and $T_{g,elas}$. To test this hypothesis, we have plotted $T_{g,elas}$ as a function of $T_{g,vis}$ in Figure 7(b). There is indeed a strong linear correlation between $T_{g,vis}$ and $T_{g,elas}$ (R^2 = 0.992), but $T_{g,elas}$ is around 50 °C lower than $T_{g,vis}$. The glass transition temperature, as measured by DSC, increases with increasing heating rate [37], but here we applied a relatively rapid heating rate of 50 °C/min so any error associated with the cooling rate should be in the opposite direction. This suggests that the Brillouin measurements of the elastic moduli probe a different frequency response in the glass structure compared to what is governing the glass transition. This is rather surprising, as the Brillouin measurements probe high frequency modes and T_g is expected to increase with

frequency. However, this result makes sense if we consider the localization of modes at higher frequency, i.e., owing to their lower activation barrier, localized secondary relaxation modes are known to "freeze in" at lower temperatures compared to the primary relaxation mechanism that are governed by cooperative flow [8]. For the eight glasses under study, $T_{g,elas}$ corresponds to an extrapolated logarithmic viscosity of 14.4±0.5 (η in Pa s) in average, i.e., to an even higher viscosity than that at the strain point of the glass ($\eta = 10^{13.68}$ Pa s). $T_{g,elas}$ have previously been compared with other measures of the glass transition temperature for different glass systems [43,70,71]. For example, Rouxel [43] found that the glass transition temperature from elastic moduli was lower than that obtained from dilatometry at the same heating rate, in qualitative agreement with the results reported here.

B. Composition and temperature dependence of Poisson's ratio

Poisson's ratio (v) is a good metric for comparing the performance of elastically strained materials and it also exhibits important relationships with densification, connectivity, ductility, and toughness [72,73]. v reflects the resistance that a material opposes to volume change with respect to shape change. Glasses typically exhibit a value of v between 0.1 and 0.4, which is correlated with the degree of glass network connectivity [43,74,75], as the short range order governs the glass network compactness and dimensionality. v generally increases with increasing atomic network packing density and decreases with increasing average coordination number [43]. Here, we have found that v increases with x, i.e., with increasing $[Al_2O_3]/[SiO_2]$ ratio (Fig. 5(a)). As the concentration of Al_2O_3 increases, the concentration of non-bridging oxygens decreases since aluminum enters the network in four-fold coordination requiring charge-compensation from an alkali or alkaline earth cation [76-80]. This causes the atomic packing density to increase along with v.

Poisson's ratio depends not only on glass composition, but also on temperature since the elastic moduli themselves are sensitive to temperature. v generally increases with temperature, as the glassy state gets closer to the liquid state [43,72,81]. For the eight glasses studied here, we have found a continuous increase of v with temperature through the glass transition (Fig. 5(b)). A sudden change would have indicated a rapid breakdown of the glass network, as it is the case for glassy B_2O_3, for which the network connectivity strongly decreases above T_g [82,83]. As noted by Rouxel [43], addition of SiO_2 enhances the three-dimensional

polymerization and the temperature sensitivity of v is reduced [84]. In the aluminosilicate glasses studied here, the increase of v with temperature is diminished at higher concentrations of Al_2O_3 (Fig. 5(c)). This is in agreement with the fact that network connectivity increases as Al_2O_3 is substituted for SiO_2.

C. Test of the shoving model

In order to test the applicability of the shoving model (Eq. (2)) for our aluminosilicate systems, we need to obtain the temperature dependence of the *instantaneous* shear modulus. This is possible from the transverse modes probed in Brillouin light scattering measurements, which provide data in the GHz range such that the measured elastic moduli can thus be understood as the frequency-independent "solid-like" moduli (also for the supercooled liquids within the considered temperature range). As a first test of the elastic shoving model, we compare the room temperature shear modulus with the glass transition temperature obtained from viscometry. According to Nemilov [85,86], elastic moduli and T_g should be proportional for chemically closely related glasses. Such proportionality has previously been reported for various glass families [43,85-88]; however, we note that one can easily find glasses with very different T_g values but the same value of E or G when the systems are chemically different, as elastic moduli reflect a mean volume density of energy, whereas T_g is related to a mean atomic bonding energy regardless of the network packing density [43]. However, as long as the glasses are chemically similar and thus have the same average intermolecular distance [55], the proportionality is usually observed. Here, we have found a relatively strong correlation (R^2 = 0.87) between G at room temperature and $T_{g,vis}$ for the aluminosilicate glasses (Fig. 8), in agreement with the elastic models.

To test the shoving model directly, we combine Eqs. (1) and (2) to determine whether the measured $G_\infty(T)$ data can reproduce the measured $\eta(T)$ data, taking V_c as the sole fitting parameter. We only use the equilibrium viscosity and moduli data, i.e., only data for temperatures above $T_{g,vis}$. Figure 9 shows the viscosities for two example glasses calculated from Eq. (12) using the optimized values of $T_{g,vis}$, m, and η_∞ for each composition. The viscosities are calculated at the same temperatures for which we have the G_∞ data available. Then the V_c parameter is optimized to calculate $\eta(T)$ based on the measured $G_\infty(T)$ data for each composition. The data illustrated in Figure 9 are for the two glasses exhibiting the best (x = 0, M = Mg) and

the worst (x = 24, M = Ca) agreement with the shoving model. We generally find good qualitative agreement with the shoving model, but there is a systematic deviation for the eight glasses, viz., the shoving model always predicts a less steep ("stronger") viscosity curve than that observed in the experimental viscosity measurements. This is also illustrated in Figures 10(a-b), in which an Angell plot of $\log_{10}\eta$ versus $T_{g,vis}/T$ is shown for two of the investigated systems. The solid lines represent the fitted MYEGA model of viscosity, whereas the data points represent the calculated viscosities based on the shoving model using the fitted value of V_c. Please note that V_c was determined using only the data for $T>T_{g,vis}$ (i.e., for equilibrium viscosities), but it was assumed temperature-independent and used to calculate viscosities also for $T<T_{g,vis}$. When the MYEGA model is extrapolated to temperatures below the glass transition, it predicts much higher viscosities than those predicted by the shoving model and those observed experimentally [10], as the viscosity is no longer an equilibrium property for $T<T_{g,vis}$. Hence, the viscous flow behavior predicted by the shoving model for $T<T_{g,vis}$ is in qualitative agreement with the experimental observations. A quantitative evaluation of the shoving model in the nonequilibrium regime ($T<T_{g,vis}$) will be the subject of an ensuing study.

As mentioned above, the shoving model predicts a lower fragility of the glass-forming liquids than that observed experimentally. This may be because the influence of entropy on liquid fragility is not accounted for in the shoving model, since the activation barrier for viscous flow (which controls fragility) is assumed to be a purely elastic energy. However, the viscous flow of glass-forming liquids is intimately linked to the configurational entropy of the liquid, which is the essence of the Adam-Gibbs (AG) viscosity model [17]. While not derived rigorously from fundamental physics, the Adam-Gibbs equation has met with remarkable success in fitting experimental data for various systems [4,89-91]. According to the AG model, the temperature dependence of viscous flow processes is governed by the temperature dependence of the size of the cooperatively rearranging region and to the height of the potential energy hindering the cooperative rearrangement of the structural units involved in the process. There have subsequently been a large number of studies confirming the intimate connection between fragility and entropy [34,92-95]. For example, Gupta and Mauro [92] derived an analytical expression showing that liquid fragility depends on the change in configurational entropy. This was later applied in topological constraint theory [96-102], from which the

composition dependence of liquid fragility can be predicted with the temperature derivative of configurational entropy as the scaling parameter [39,103-105].

We have used the proportionality constant V_c between $G_\infty(T)$ and $\Delta F(T)$) as the fitting parameter. This "characteristic" volume is not equal to the volume change during the flow event (shoving), which is instead the activation volume (ΔV). For small activation volume, V_c is given by [51]

$$V_c = \frac{2}{3}\frac{\Delta V^2}{V}, \tag{13}$$

where V is the volume of the flowing region before flow. We have compared the fitted value of V_c for each composition to the molar volume of the glass (V_m). V_m is calculated based on the room temperature density and the analyzed chemical composition. It appears that V_c is composition-dependent, since it becomes larger with increasing molar volume (Fig. 11). This result suggests an intimate connection between the volume associated with the flow event and the openness of the glass structure, viz., when the glass structure is more open, a larger volume is involved in the shoving.

V. CONCLUSIONS

We have presented the first systematic comparison of the evolution of shear moduli both well below and slightly above T_g with shear viscosity data for oxide glass systems. Specifically, we have studied a series of sodium aluminosilicate compositions with MgO and/or CaO. Dyre's shoving model of the glass transition is partially supported by our data, but the model systematically predicts a less steep ("stronger") viscosity curve than what is observed experimentally, suggesting that the dynamics of the glass transition are governed by additional factors beyond the evolution of the shear modulus. Around 70% of the variation of the characteristic volume of the shoving event can be explained by the variation of the molar volume of the glass at room temperature. We have also found that the increase in Poisson's ratio with temperature is diminished at high concentrations of Al_2O_3, since the network connectivity increases as Al_2O_3 is substituted for SiO_2. Finally, we have compared the glass transition temperature $T_{g,vis}$ obtained from viscosity (temperature at 10^{12} Pa s) with the onset temperatures of the decrease in elastic moduli ($T_{g,elas}$) and increase in the thermal expansion coefficient ($T_{g,CTE}$) during heating. While we find an approximate one-to-one correlation between

$T_{g,vis}$ and $T_{g,CTE}$, we note that the elastic moduli probe a different frequency response of the glass structure since $T_{g,elas}$ is systematically lower than $T_{g,vis}$.

ACKNOWLEDGEMENTS

We thank the Advanced Materials Processing Laboratory and Characterization Sciences and Services Directorate at Corning Incorporated for help with glass preparation and characterization, respectively. We are also thankful for valuable discussions with Marcel Potuzak of Corning Incorporated. L. Huang acknowledges the National Science Foundation for the financial support under Grant No. DMR-907076.

REFERENCES

1. G. W. Scherer, *Relaxation in Glass and Composites* (John Wiley & Sons, New York, 1986).
2. P. G. Debenedetti, *Metastable Liquids: Concepts and Principles* (Princeton University Press, Princeton, 1996).
3. P. G. Debenedetti and F. H. Stillinger, Nature **410**, 259 (2001).
4. M. D. Ediger, C. A. Angell, and S. R. Nagel, J. Phys. Chem. **100**, 13200 (1996).
5. J. C. Dyre, J. Non-Cryst. Solids **235-237**, 142 (1998).
6. C. A. Angell, J. Non-Cryst. Solids **102**, 205 (1988).
7. C. A. Angell, J. Non-Cryst. Solids **131-133**, 13 (1991).
8. C. A. Angell, K. L. Ngai, G. B. McKenna, P. F. McMillan, and S. W. Martin, J. Appl. Phys. **88**, 3113 (2000).
9. J. C. Mauro and R. J. Loucks, Phys. Rev. B **76**, 174202 (2007).
10. J. C. Mauro, D. C. Allan, and M. Potuzak, Phys. Rev. B **80**, 094204 (2009).
11. J. C. Mauro, P. K. Gupta, and R. J. Loucks, J. Chem. Phys. **126**, 184511 (2007).
12. P. K. Gupta and J. C. Mauro, J. Chem. Phys. **126**, 224504 (2007).
13. J. C. Mauro, R. J. Loucks, and S. Sen, J. Chem. Phys. **133**, 164503 (2010).
14. J. C. Mauro, Int. J. Appl. Glass Sci. **2**, 245 (2011).
15. M. L. Williams, R. F. Landel, and J. D. Ferry, J. Am. Chem. Soc. **77**, 3701 (1955).
16. W. T. Laughlin and D. R. Uhlmann, J. Phys. Chem. **76**, 2317 (1972).
17. G. Adam and J. H. Gibbs, J. Chem. Phys. **43**, 139 (1965).
18. T. Hecksher, A. I. Nielsen, N. B. Olsen, and J. C. Dyre, Nat. Phys. **4**, 737 (2008).
19. J. C. Mauro, Y. Z. Yue, A. J. Ellison, P. K. Gupta, and D. C. Allan, Proc. Natl. Acad. Sci. (U.S.) **106**, 19780 (2009).
20. R. Richert and C. A. Angell, J. Chem. Phys. **108**, 9016 (1998).
21. C. A. Angell, J. Phys.: Cond. Matter **12**, 6463 (2000).
22. I. Avramov, J. Non-Cryst. Solids **351**, 3163 (2005).
23. J. C. Dyre, J. Phys.: Cond. Matter **19**, 205105 (2007).
24. M. I. Ojovan, K. P. Travis, and R. J. Hand, J. Phys.: Cond. Matter **19**, 415107 (2007).
25. J. C. Mauro and R. J. Loucks, Phys. Rev. E **78**, 021502 (2008).
26. C. Z. Zhang, L. N. Hu, Y. Z. Yue, and J. C. Mauro, J. Chem. Phys. **133**, 014508 (2010).
27. A. K. Varshneya, *Fundamentals of Inorganic Glasses*, 2nd ed. (Society of Glass Technology, Sheffield, 2006).

28. G. G. Naumis, Phys. Rev. B **61**, R9205 (2000).
29. K. Trachenko, Phys. Rev. B **78**, 104201 (2008).
30. K. Trachenko and V. V. Brazhkin, Phys. Rev. B **83**, 014201 (2011).
31. H. E. Stanley and J. Teixeira, J. Chem. Phys. **73**, 3404 (1980).
32. U. Buchenau and A. Wischnewski, Phys. Rev. B **70**, 092201 (2004).
33. Y. Z. Yue, J. Non-Cryst. Solids **354**, 1112 (2008).
34. Y. Z. Yue, J. Non-Cryst. Solids **355**, 737 (2009).
35. X. J. Guo, M. Potuzak, J. C. Mauro, D. C. Allan, T. J. Kiczenski, and Y. Z. Yue, J. Non-Cryst. Solids **357**, 3230 (2011).
36. C. T. Moynihan, A. J. Easteal, D. C. Tran, J. A. Wilder, and E. P. Donovan, J. Am. Ceram. Soc. **59**, 137 (1976).
37. C. T. Moynihan, S.-K. Lee, M. Tatsumisago, and T. Minami, Thermochim. Acta **280-281**, 153 (1996).
38. V. Velikov, S. Borick, and C. A. Angell, Science **294**, 2335 (2001).
39. M. M. Smedskjaer, J. C. Mauro, R. E. Youngman, C. L. Hogue, M. Potuzak, and Y. Z. Yue, J. Phys. Chem. B **115**, 12930 (2011).
40. R. Roy, D. K. Agrawal, and H. A. McKinstry, Annu. Rev. Mater. Sci. **19**, 59 (1989).
41. M. Potuzak, J. C. Mauro, T. J. Kiczenski, A. J. Ellison, and D. C. Allan, J. Chem. Phys. **133**, 091102 (2010).
42. R. M. C. V. Reis, J. C. Mauro, K. L. Geisinger, M. Potuzak, M. M. Smedskjaer, X. J. Guo, and D. C. Allan, J. Non-Cryst. Solids **358**, 648 (2012).
43. T. Rouxel, J. Am. Ceram. Soc. **90**, 3019 (2007).
44. R. E. Youngman, J. Kieffer, J. D. Bass, and L. Duffrene, J. Non-Cryst. Solids **222**, 190 (1997).
45. T. Rouxel, C. R. Mecanique **334**, 743 (2006).
46. J. E. Masnik, J. Kieffer, and J. D. Bass, J. Chem. Phys. **103**, 9907 (1995).
47. M. H. Cohen and D. Turnbull, J. Chem. Phys. **31**, 1164 (1959).
48. D. Turnbull and M. H. Cohen, J. Chem. Phys. **34**, 120 (1961).
49. G. S. Grest and M. H. Cohen, Adv. Chem. Phys. **48**, 455 (1981).
50. J. H. Gibbs and E. A. DiMarzio, J. Chem. Phys. **28**, 373 (1958).
51. J. C. Dyre, N. B. Olsen, and T. Christensen, Phys. Rev. B **53**, 2171 (1996).
52. N. B. Olsen, J. C. Dyre, and T. Christensen, Phys. Rev. Lett. **81**, 1031 (1998).

53. J. C. Dyre and N. B. Olsen, Phys. Rev. E **69**, 042501 (2004).

54. J. C. Dyre, T. Christensen, and N. B. Olsen, J. Non-Cryst. Solids **352**, 4635 (2006).

55. J. C. Dyre, Rev. Mod. Phys. **78**, 953 (2006).

56. G. Wyllie, Phys. Rep. **61**, 329 (1980).

57. B. Xu and G. B. McKenna, J. Chem. Phys. **134**, 124902 (2011).

58. D. H. Torchinsky, J. A. Johnson, and K. A. Nelson, J.Chem. Phys. **130**, 064502 (2009).

59. A. S. Bains, C. A. Gordon, A. V. Granato, and R. B. Schwarz, J. Alloys Compd. **310**, 20 (2001).

60. V. A. Khonik, Yu. P. Mitrofanov, S. A. Lyakhov, A. N. Vasiliev, S. V. Khonik, and D. A. Khoviv, Phys. Rev. B **79**, 132204 (2009).

61. F. Puosi and D. Leporini, J. Chem. Phys. **136**, 041104 (2012).

62. M. M. Smedskjaer, S. A. Saxton, A. J. Ellison, and J. C. Mauro, Opt. Lett. **37**, 293 (2012).

63. G. G. Naumis, J. Non-Cryst. Solids **352**, 4865 (2006).

64. C. A. Angell, Science **267**, 1924 (1995).

65. J. K. Russell, D. Giordano, and D. B. Dingwell, Am. Mineral. **88**, 1390 (2003).

66. D. Giordano, J. K. Russell, and D. B. Dingwell, Earth Plan. Sci. Lett. **271**, 123 (2008).

67. Q. J. Zheng, J. C. Mauro, A. J. Ellison, M. Potuzak, and Y. Z. Yue, Phys. Rev. B **83**, 212202 (2011).

68. K. Levenberg, Quart. Appl. Math. **2**, 164 (1944).

69. D. Marquardt, J. Soc. Indust. Appl. Math. **11**, 431 (1963).

70. D. Vo-Thanh, Y. Bottinga, A. Polian, and P. Richet, J. Non-Cryst. Solids **351**, 61 (2005).

71. A. Hushur, S. Kojima, M. Kodama, B. Whittington, M. Olesiak, M. Affatigato, and S. A. Feller, Jpn. J. Appl. Phys. **44**, 6683 (2005).

72. G. N. Greaves, A. L. Greer, R. S. Lakes, and T. Rouxel, Nat. Mater. **10**, 823 (2011).

73. L. Wondraczek, J. C. Mauro, J. Eckert, U. Kühn, J. Horbach, J. Deubener, and T. Rouxel, Adv. Mater. **23**, 4578 (2011).

74. B. Bridge, N. D. Patel, and D. N. Waters, Phys. Stat. Sol. A **77**, 655 (1983).

75. B. Bridge and A. A. Higazy, Phys. Chem. Glasses **27**, 1 (1986).

76. J. C. C. Chan, M. Bertmer, and H. Eckert, J. Am. Chem. Soc. **121**, 5238 (1999).

77. F. Seifert, B. O. Mysen, and D. Virgo, Am. Mineral. **67**, 696 (1982).

78. S. H. Risbud, R. J. Kirkpatrick, A. P. Taglialavore, and B. Montez, J. Am. Ceram. Soc. **70**, C10 (1987).

79. M. J. Toplis, S. C. Kohn, M. E. Smith, and I. J. F. Poplett, Am. Mineral. **85**, 1556 (2000).

80. S. Sen and R. E. Youngman, J. Phys. Chem. B **108**, 7557 (2004).

81. Y. Gueguen, T. Rouxel, P. Gadaud, C. Bernard, V. Keryvin, and J.-C. Sangleboeuf, Phys. Rev. B **84**, 064201 (2011).

82. J. Kieffer, Phys. Rev. B **50**, 17 (1994).

83. A. K. Hassan, L. M. Torell, L. Börjesson, and H. Doweidar, Phys. Rev. B **45**, 12797 (1992).

84. S. Spinner, J. Am. Ceram. Soc. **39**, 113 (1956).

85. S. V. Nemilov, Sov. J. Glass Phys. Chem. **18**, 1 (1992).

86. S. V. Nemilov, *Thermodynamics and Kinetic Aspects of the Vitreous State* (CRC, Boca Raton, 1995).

87. W. H. Wang, J. Non-Cryst. Solids **351**, 1481 (2005).

88. W. H. Wang, J. Appl. Phys. **99**, 093506 (2006).

89. G. W. Scherer, J. Am. Ceram. Soc. **67**, 504 (1984).

90. R. Richert and C. A. Angell, J. Chem. Phys. **108**, 9016 (1998).

91. C. M. Roland, S. Capaccioli, M. Lucchesi, and R. Casalini, J. Chem. Phys. **120**, 10640 (2004).

92. P. K. Gupta and J. C. Mauro, Phys. Rev. E **78**, 062501 (2008).

93. R. J. Speedy, J. Phys. Chem. B **103**, 4060 (1999).

94. S. Sastry, Nature **409**, 164 (2001).

95. L.-M. Martinez and C. A. Angell, Nature **410**, 663 (2001).

96. J. C. Phillips, J. Non-Cryst. Solids **34**, 153 (1979).

97. M. F. Thorpe, J. Non-Cryst. Solids **57**, 355 (1983).

98. P. Boolchand, G. Lucovsky, J. C. Phillips, and M. F. Thorpe, Philos. Mag. **85**, 3823 (2005).

99. G. G. Naumis, Phys. Rev. E **71**, 026114 (2005).

100. M. Micoulaut and J. C. Phillips, J. Non-Cryst. Solids **353**, 1732 (2007).

101. M. Micoulaut, J. Phys.: Cond. Matt. **22**, 285101 (2010).

102. J. C. Mauro, Am. Ceram. Soc. Bull. **90** [4], 31 (2011).

103. P. K. Gupta and J. C. Mauro, J. Chem. Phys. **130**, 094503 (2009).

104. J. C. Mauro, P. K. Gupta, and R. J. Loucks, J. Chem. Phys. **130**, 234503 (2009).

105. M. M. Smedskjaer, J. C. Mauro, S. Sen, and Y. Z. Yue, Chem. Mater. **22**, 5358 (2010).

FIGURES

FIG. 1. (Color online) (a) Logarithmic shear viscosity ($\log_{10}\eta$) as a function of the absolute temperature (T) for the glass with x = 0, M = Ca. The data are fit with the MYEGA model of Eq. (12) to obtain the glass transition temperature at 10^{12} Pa s ($T_{g,vis}$). (b) Composition dependence of $T_{g,vis}$ for the Ca- and Mg-glasses. Inset: composition dependence of $T_{g,vis}$ for the mixed Ca-Mg glasses with x = 16. The uncertainty of $T_{g,vis}$ is approximately ±2 °C.

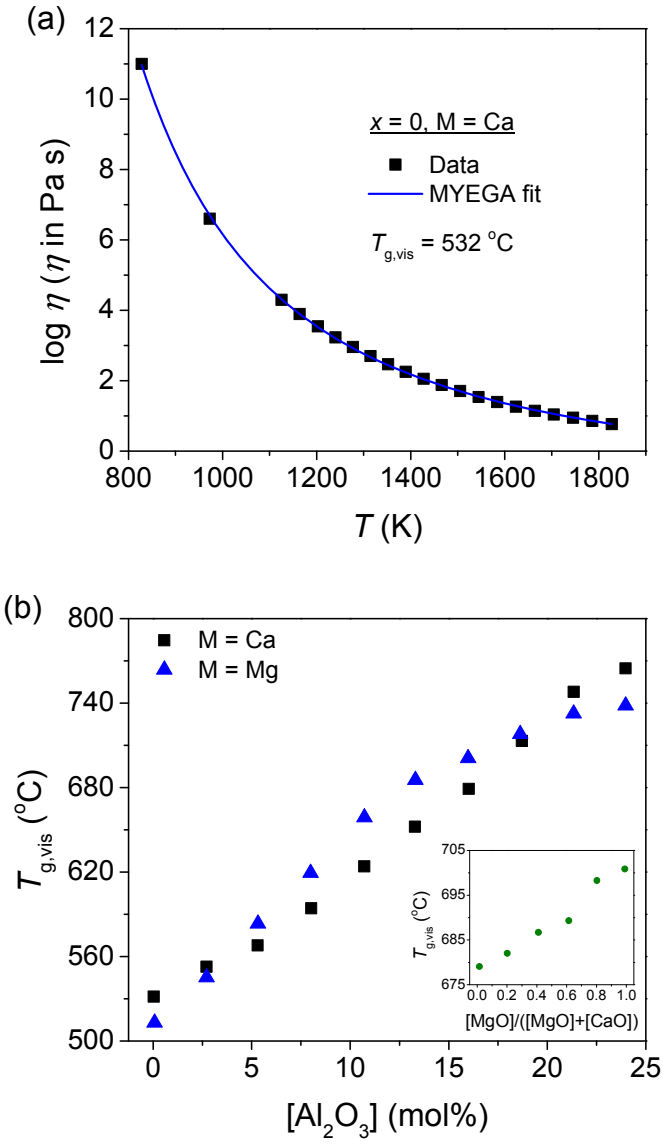

FIG. 2. (Color online) Temperature dependence of Young's modulus (E) as determined by Brillouin light scattering experiments for both (a) Ca-glasses and (b) Mg-glasses. The uncertainty of E is approximately ±0.2 GPa.

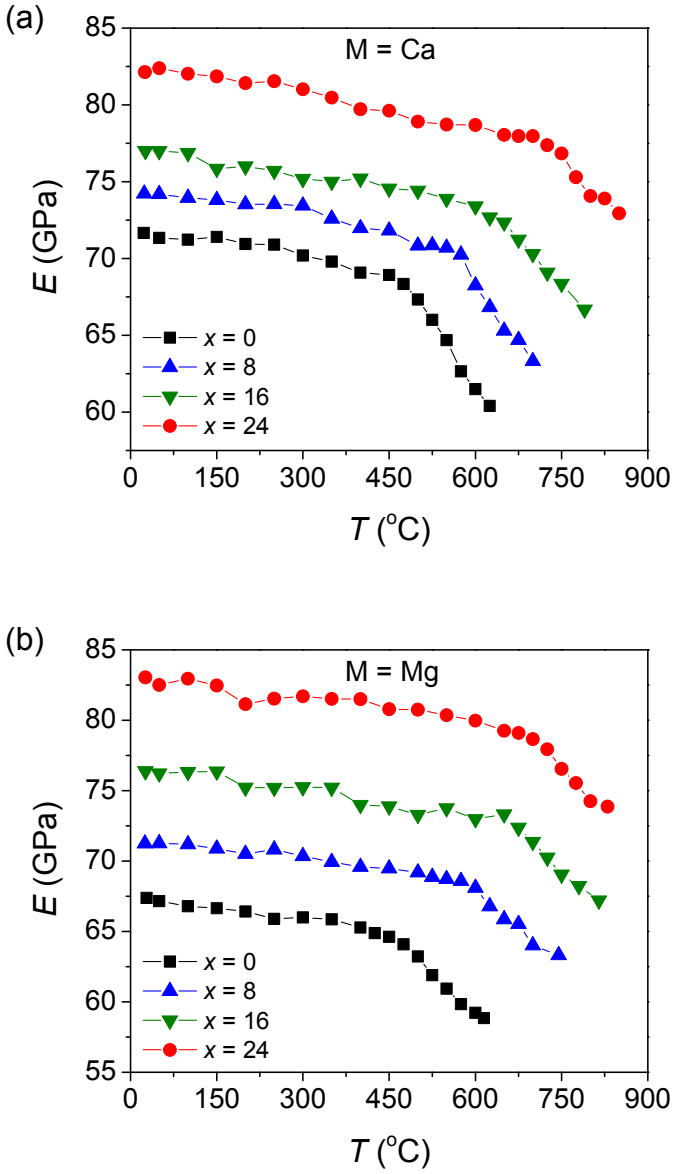

FIG. 3. (Color online) Temperature dependence of shear modulus (G) as determined by Brillouin light scattering experiments for both (a) Ca-glasses and (b) Mg-glasses. The uncertainty of G is approximately ±0.2 GPa.

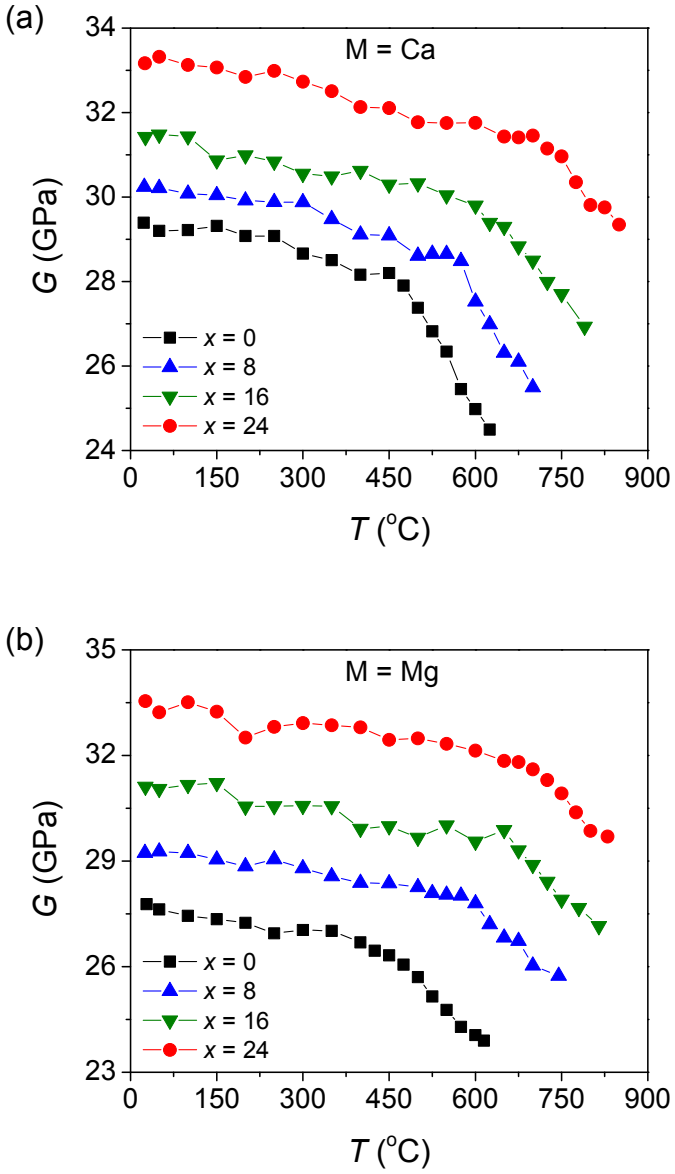

FIG. 4. (Color online) (a) Illustration of the procedure for determining the glass transition temperature $T_{g,elas}$ based on $G(T)$ data from Brillouin light scattering experiments. The shown curve is for the glass with $x = 0$ and M = Ca. (b) Composition dependence of $T_{g,elas}$ for the Ca- and Mg-glasses. The uncertainty of $T_{g,elas}$ is estimated to be around ±5 °C.

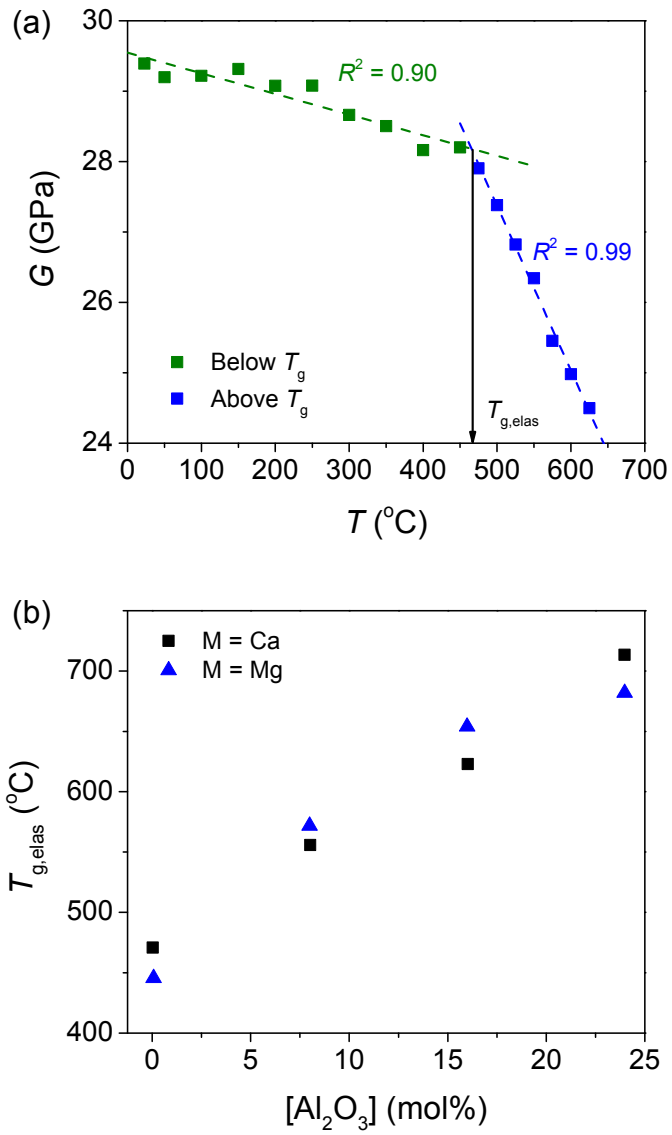

FIG. 5. (Color online) (a) Composition dependence of Poisson's ratio (v) at room temperature. (b) Temperature dependence of Poisson's ratio for the glass with $x = 0$ and M = Ca. (c) Composition dependence of the slope of the v vs. T curve for the eight studied glasses (dv/dT).

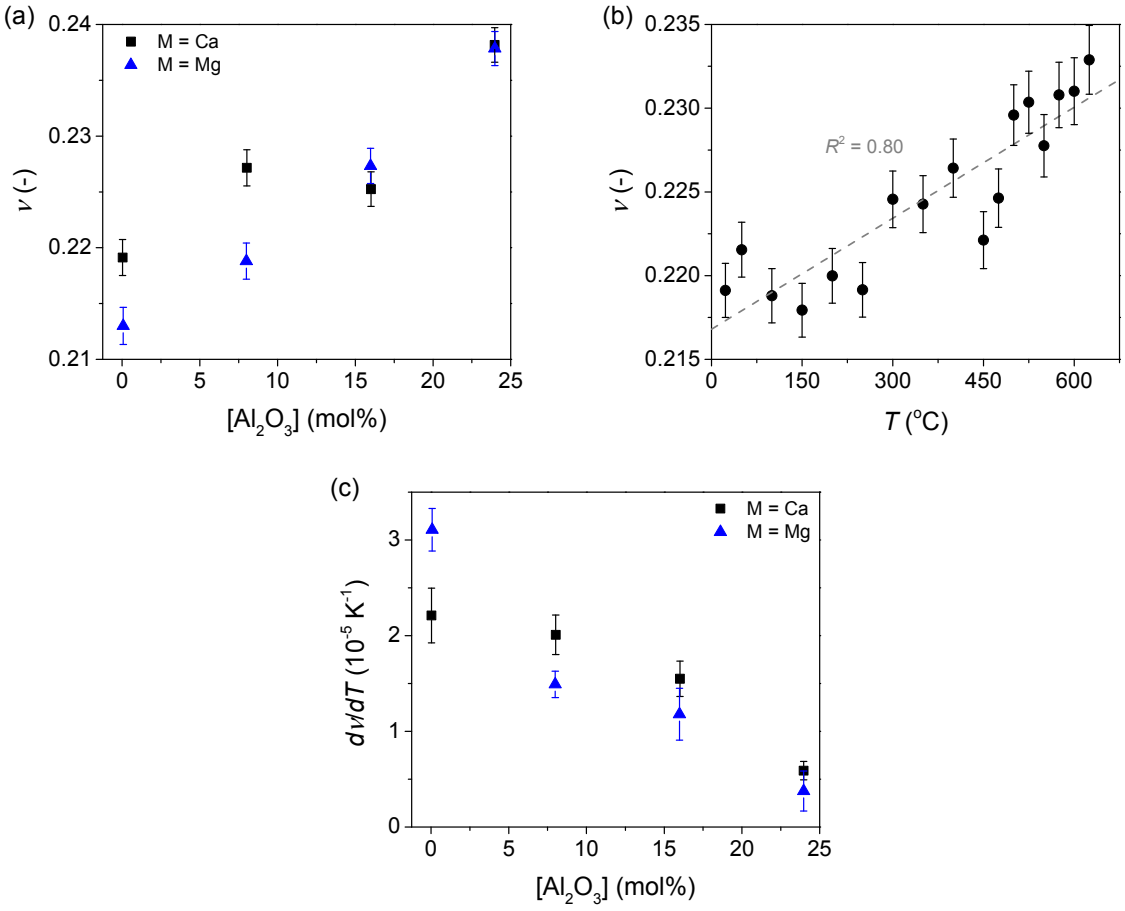

FIG. 6. (Color online) (a) Illustration of the procedure for determining the glass transition temperature $T_{g,CTE}$ based on the high-temperature thermal expansion measurements. The primary y-axis gives the thermal expansion, whereas the secondary y-axis gives the instantaneous CTE. The data are for the glass with $x = 0$ and M = Ca. (b) Composition dependence of $T_{g,CTE}$ for the Ca- and Mg-glasses. The uncertainty of $T_{g,CTE}$ is estimated to be around ±5 °C.

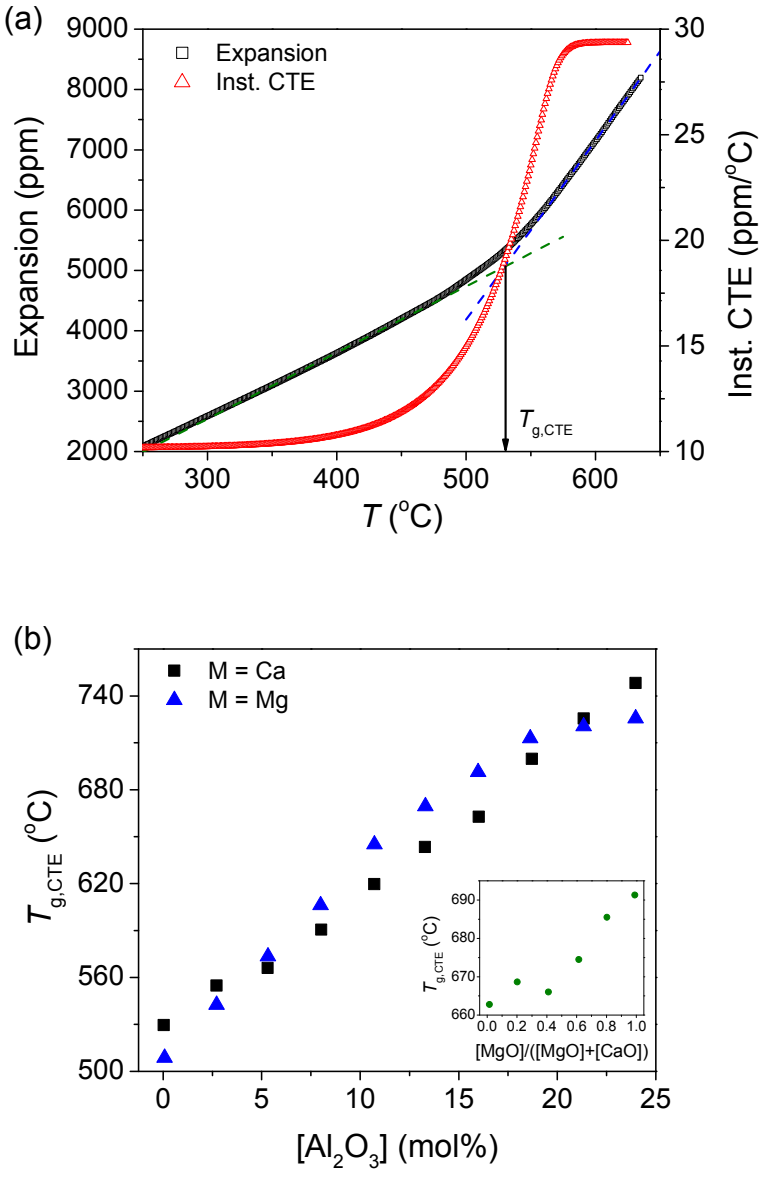

FIG. 7. (Color online) Comparison of $T_{g,vis}$ with (a) $T_{g,CTE}$ and (b) $T_{g,elas}$. The dashed lines represent linear fits to the data. The red solid lines represent the lines through $T_{g,CTE} = T_{g,vis}$ and $T_{g,elas} = T_{g,vis}$, respectively.

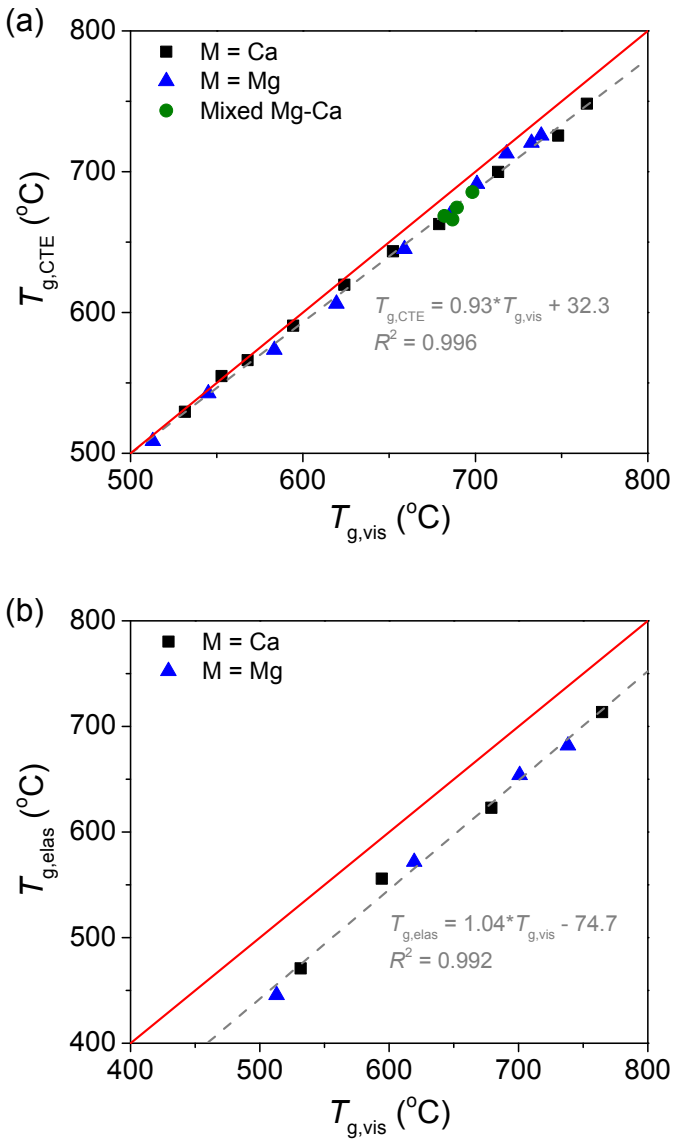

FIG. 8. (Color online) Shear modulus (G) at room temperature as a function of the glass transition temperature at 10^{12} Pa s ($T_{g,vis}$).

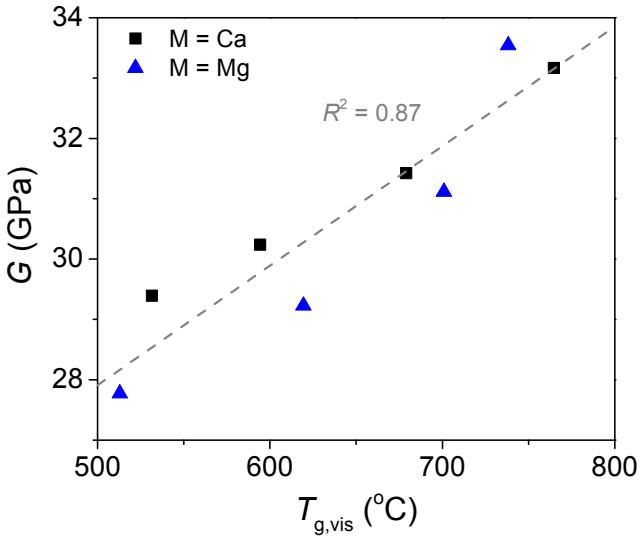

FIG. 9. (Color online) Logarithmic shear viscosity ($\log_{10}\eta$) as a function of the absolute temperature (T) for the glasses with x = 0, M = Mg and x = 24, M = Ca. The viscosities are calculated from the MYEGA fit (Eq. (12)) at the temperatures for which the Brillouin light scattering experiments were performed (solid symbols). The viscosities are then predicted using the shoving model (Eq. (2)) and the measured shear moduli taking the temperature-independent volume (V_c) as the sole fitting parameter (open symbols).

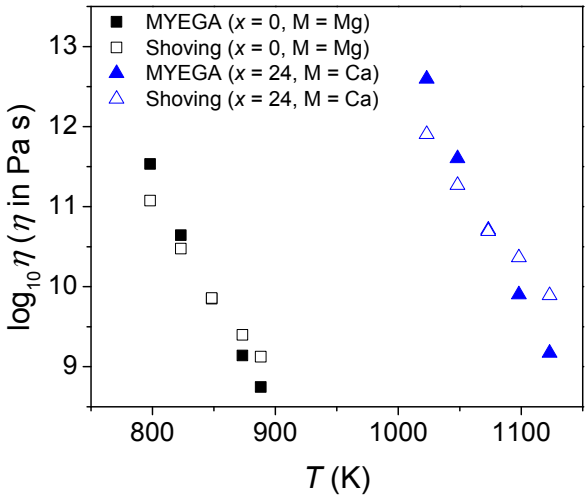

FIG. 10. (Color online) Angell fragility plot showing the logarithmic shear viscosity ($\log_{10}\eta$) as a function of the $T_{g,vis}$ scaled inverse temperature ($T_{g,vis}/T$) for the glasses with (a) x = 0, M = Ca and (b) x = 0, M = Mg. The solid lines represent the MYEGA model for equilibrium viscosity (Eq. (12)) with the fitted values of $T_{g,vis}$, m, and η_∞ for this glass. The data points are the predicted values of η using the shoving model (Eq. (2)) combined with the measured temperature dependence of shear modulus.

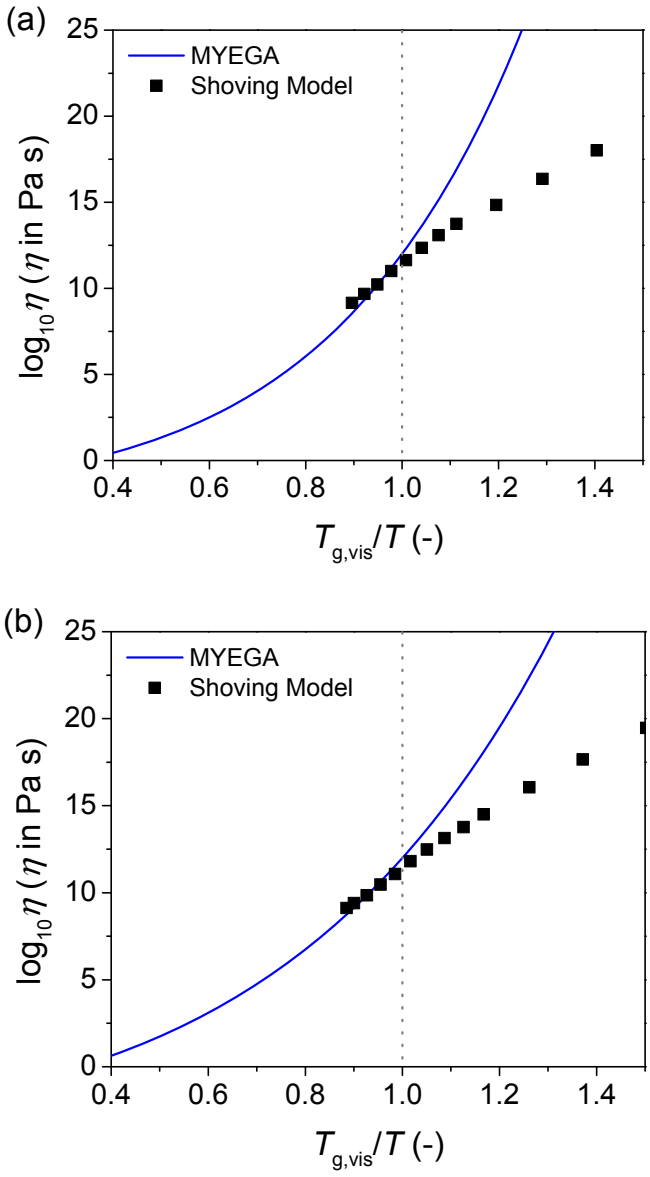

FIG. 11. (Color online) The fitted value of the temperature-independent microscopic volume (V_c) as a function of the molar volume of the glasses at room temperature (V_m).